Could CO_2-induced land-cover feedbacks alter near-shore upwelling regimes?

Noah S. Diffenbaugh*, Mark A. Snyder, and Lisa C. Sloan

Department of Earth Sciences, University of California, 1156 High Street, Santa Cruz, CA 95064

Edited by Susan Solomon, National Oceanic and Atmospheric Administration, Boulder, CO, and approved October 31, 2003 (received for review September 8, 2003)

The response of marine and terrestrial environments to global changes in atmospheric carbon dioxide (CO_2) concentrations will likely be governed by both responses to direct environmental forcing and responses to Earth-system feedbacks induced by that forcing. It has been proposed that anthropogenic greenhouse forcing will intensify coastal upwelling in eastern boundary current regions [Bakun, A. (1990) *Science* 247, 198–201]. Focusing on the California Current, we show that biophysical land-cover–atmosphere feedbacks induced by CO_2 radiative forcing enhance the radiative effects of CO_2 on land–sea thermal contrast, resulting in changes in eastern boundary current total seasonal upwelling and upwelling seasonality. Specifically, relative to CO_2 radiative forcing, land-cover–atmosphere feedbacks lead to a stronger increase in peak- and late-season near-shore upwelling in the northern limb of the California Current and a stronger decrease in peak- and late-season near-shore upwelling in the southern limb. Such changes will impact both marine and terrestrial communities [Bakun, A. (1990) *Science* 247, 198–201; Soto, C. G. (2001) *Rev. Fish Biol. Fish.* 11, 181–195; and Agostini, V. N. & Bakun, A. (2002) *Fish. Oceanogr.* 11, 129–142], and these and other Earth-system feedbacks should be expected to play a substantial role in shaping the response of eastern boundary current regions to CO_2 radiative forcing.

Near-shore upwelling regimes are important both for marine and terrestrial environments, supporting diverse and highly productive marine communities and exerting a strong control on adjacent terrestrial climate. These regimes classically occur in subtropical eastern boundary current regions, the most prominent of which are the California, Canary, Benguela, and Peru/Humbolt systems (1), at which strong seasonal along-shore winds drive offshore Ekman transport, resulting in the seasonal upwelling of cold, nutrient-rich water (2). Bakun (2) proposed that elevated atmospheric CO_2 concentrations could intensify coastal ocean upwelling by heating the land surface more than the ocean, enhancing the spring and summer land–sea contrast that drives near-shore upwelling in eastern boundary current regions. Although comprehensive observations of coastal upwelling are not available, this hypothesis has been supported by analyses of observed upwelling indicators showing positive trends since the mid-20th century (2, 3). Global-scale numerical experiments have had limited success capturing this effect (4). However, by using a high-resolution regional climate model (RCM), Snyder *et al*. (5) have shown that both the seasonality and peak strength of upwelling in the California Current are sensitive to elevated CO_2 concentrations, with radiative forcing resulting in an intensified peak season in the northern limb and a muted peak season in the southern limb.

Although there has been brief consideration of the potential role that increased upwelling could play in mitigating the elevation of atmospheric CO_2 levels through biogeochemical feedbacks (2), neither the original hypothesis nor any of the subsequent studies have considered the potential effects of Earth-system feedbacks on the response of coastal upwelling regimes to greenhouse forcing. One such feedback could occur between land cover and the atmosphere as plant communities respond to elevated atmospheric CO_2 concentrations. The importance of land-cover change in shaping regional and global climates has been firmly established, both for changes in land use and changes in equilibrium vegetation distribution (6–10). Indeed, it has been shown that on a regional basis the relative magnitudes of climate sensitivity to Industrial Age changes in land-cover and atmospheric CO_2 concentration are similar (11). Plant distributions will likely be highly sensitive to the climatic and physiological effects of future increases in atmospheric CO_2 (12), and changes in land cover due to these sensitivities could feed back through land-cover–atmosphere interactions to alter the climate system further, potentially enhancing or dampening the effects of CO_2 radiative forcing on coastal upwelling regimes.

The original hypothesis of Bakun (2) that CO_2 radiative forcing could intensify coastal upwelling through the differential response of surface temperature and pressure over land and ocean has been strengthened by the results of Snyder *et al*. (5), who quantified the effect of projected 21st-century CO_2 concentrations on the seasonal structure of the land–sea temperature contrast over western North America and the eastern Pacific, as well as the effect of this change in land–sea contrast on the seasonal structure of California Current activity. Given this sensitivity, how might land-cover–atmosphere feedbacks induced by anthropogenically elevated atmospheric CO_2 concentrations alter the upwelling response? Doubling of preindustrial atmospheric CO_2 concentrations has been projected to create warmer, dryer conditions on land in eastern boundary current regions (12, 13). This change in climate would likely increase heat and water stress for existing vegetation, creating more sparse vegetation cover, decreasing soil moisture and evapotranspiration, increasing surface-sensible heat flux, and further increasing temperatures on land. CO_2-induced changes in land cover could also alter surface reflectivity (albedo), which in turn could alter surface energy balance. If such feedbacks were to enhance the radiative effects of CO_2 by further warming the land and enhancing land–sea temperature contrast, the effect on near-shore upwelling regimes would be even more severe than that proposed by Bakun (2) and quantified by Snyder *et al*. (5).

To test the effect of CO_2-induced land-cover–atmosphere feedbacks on coastal upwelling regimes, we focused on the California Current, an eastern boundary current that flows southward along the west coast of North America. The northern and southern limbs of the California Current exhibit distinct seasonal structures, with a much more pronounced peak season and greater seasonal contrast north of the Southern California Bight (34.5°N) (1). The nutrient-rich water upwelled in the California Current supports a highly productive and complex polytrophic marine ecosystem including economically important fishery resources (2, 14). Onshore, California Current activity directly impacts terrestrial environments, particularly through

This paper was submitted directly (Track II) to the PNAS office.

Abbreviations: RCM, regional climate model; RegCM*n*, Regional Climate Model, version *n*; ppmv, ppm by volume.

*To whom correspondence should be addressed. E-mail: ndiffenbaugh@es.ucsc.edu.

the coastal fog regime produced by near-shore upwelling activity. The distinct coastal redwood forests of northern California and southern Oregon depend on this fog regime for spring and summer moisture, and the range of the coast redwood is tied closely to the along-shore extent of the northern limb of the California Current (15).

Methods

Models. To test the sensitivity of California Current activity to CO_2-induced land-cover–atmosphere feedbacks, we used three numerical Earth-system models: the National Center for Atmospheric Research Community Climate Model, version 3.6.6 (16); the National Center for Atmospheric Research Regional Climate Model, version 2.5 (RegCM2.5) (5, 12, 13, 17–19); and BIOME4 (20), an equilibrium vegetation model. We used the Community Climate Model/RegCM2.5 grid and configuration described by Snyder *et al*. (18) and the RegCM2.5/BIOME4 configuration described by Diffenbaugh *et al*. (12). RegCM2.5 has been used to study a variety of climate problems in a variety of regions and has been well validated in the California Current region (13, 18, 19). Additionally, BIOME4 performs well in simulating the biogeography of the western United States when driven by the observed regional climatology (12). Driven by RegCM2.5 output from the CONTROL case (described below), BIOME4 also reproduces the general biogeography of the region, with temperate conifer forest along the coast of northern California and southern Oregon, a mix of temperate grassland, temperate shrubland and desert in the Great Basin and Desert Southwest, and cool and cold conifer and mixed forests in the high elevations of the Mountain West (data not shown). In the control RegCM2.5/BIOME4 coupling, temperate conifer forest is underrepresented on the coast of central California and northern Oregon, and temperate shrubland is overrepresented in central and southern California.

Asynchronous Coupling. To simulate land-cover–atmosphere feedbacks, we used the asynchronous-coupling technique of de Noblet-Ducoudré *et al*. (21). To maintain fidelity between the land-cover and topography boundary conditions in the RCM, we used the "absolute" technique, in which the climate model output is used directly to drive the vegetation model, without adding simulated anomalies to an observed baseline climate data set. Net changes in simulated vegetation distribution were a result of the initial climatic and physiological effects of elevated atmospheric CO_2 concentrations as well as of the subsequent changes in climate induced by the climate model–vegetation model asynchronous coupling. In this asynchronous-coupling strategy, changes in land cover can alter the simulated climate by altering fluxes of energy, momentum, and moisture at the surface. The Biosphere–Atmosphere Transfer Scheme (22) is the land-surface component of RegCM2.5. Values of key land-surface parameters such as albedo, surface roughness, leaf-area index, and stomatal resistance are prescribed in the biosphere–atmosphere transfer scheme for each land-cover type. Changes in land cover simulated in each iteration can alter the values of these parameters at each grid point, in turn altering values of key climate variables (such as soil moisture, evaporation-and sensible heating) in subsequent iterations.

Model Cases. We compared results of three RCM cases. The CONTROL case used preindustrial atmospheric CO_2 concentrations [280 ppm by volume (ppmv)], whereas the $2XCO_2$ case, which tested the sensitivity of California Current activity to elevated CO_2 levels, used doubled preindustrial atmospheric CO_2 concentrations (560 ppmv). Both used modern potential vegetation and prescribed sea surface temperatures (SSTs) calculated in equilibrium with the respective CO_2 levels [described by Snyder *et al*. (18)]. The $2XCO_2$+VEG case tested the sensitivity of California Current activity to land-cover–atmosphere feedbacks by using the identical atmospheric CO_2 levels, SSTs, and general circulation model driver conditions as the $2XCO_2$ case but asynchronously coupling RegCM2 and BIOME4 as described above. Following Snyder *et al*. (18), the general circulation model driver was allowed 4 years for model equilibration and the RCM was allowed 3 years. In the $2XCO_2$+VEG case, we used three iterations of the RegCM2/BIOME4 asynchronous coupling, all of which used 560 ppmv of CO_2 in the BIOME4 simulation. The initial land-cover boundary condition for the $2XCO_2$+VEG case was achieved by driving BIOME4 with the final 15 model years of the $2XCO_2$ case [described by Diffenbaugh *et al*. (13)]. Thereafter, each iteration consisted of a 13-year RegCM2 model integration, with the final 10 model years used to drive the BIOME4 simulation, the results of which were used as the land-cover boundary condition in the following RegCM2 simulation. For the analyses shown here, the final 10 model years of the third iteration of the $2XCO_2$+VEG case were compared with 10 model years from the CONTROL and $2XCO_2$ cases. A buffer of eight grid points was discarded from the lateral boundary for all RegCM2.5 analyses.

The relative sensitivity of California Current activity to CO_2 radiative forcing and CO_2-induced land-cover change is reflected in the anomalies between the various climate model integrations. The only difference in boundary conditions between the CONTROL and $2XCO_2$ cases was the atmospheric CO_2 concentration (280 and 560 ppmv, respectively). Likewise, the only difference in boundary conditions between the $2XCO_2$ and $2XCO_2$+VEG cases was the vegetation distribution (preindustrial and 560-ppmv-CO_2-equilibrated, respectively). Thus, anomalies between the $2XCO_2$ and CONTROL cases ($2XCO_2$ − CONTROL) yield the sensitivity to CO_2 radiative forcing. Anomalies between the $2XCO_2$+VEG and $2XCO_2$ cases ($2XCO_2$+VEG − $2XCO_2$) yield the sensitivity to CO_2-induced land-cover change. In this methodology, we test the response of California Current activity to vegetation change in equilibrium with a particular atmospheric CO_2 value. We do not test how this response may vary with varying CO_2 concentrations.

Wind-Stress Curl. Coastal upwelling in eastern boundary current regions is driven by along-shore wind stress [see conceptual diagram by Bakun (2)]. Offshore Ekman transport of surface waters occurs perpendicular to the direction of the wind stress, with the transported surface water replaced from below. Just seaward of the coastal margin, wind-stress curl acts as the key control on Ekman pumping, with positive (cyclonic) wind-stress curl resulting in near-shore upwelling (1). The sensitivity of eastern boundary current wind-stress curl thereby serves as a measure of eastern boundary current upwelling sensitivity to changes in atmospheric CO_2 levels and CO_2-induced land-cover change. Methods for calculating wind-stress curl from RegCM2.5 output are described by Diffenbaugh *et al*. (19) and Snyder *et al*. (5). RegCM2.5 accurately simulates the seasonal cycle of wind-stress curl in the California Current [see Diffenbaugh *et al*. (19) for comparison with observed fields]. This methodology is limited to testing the sensitivity of wind-driven processes to CO_2-induced land-cover change. The role of ocean–atmosphere interactions in shaping the response of California Current activity to land-cover change was not tested.

Results and Discussion

Land-cover–atmosphere interactions simulated in the $2XCO_2$+VEG case warm the land in the late winter/early spring and in the summer, accentuating the response of the land–sea contrast seen in the $2XCO_2$ case (Fig. 1). Evaporation over land decreases in the summer months in the $2XCO_2$+VEG case, whereas sensible heating increases, with the decreases in evaporation largely associated with decreases in soil moisture and

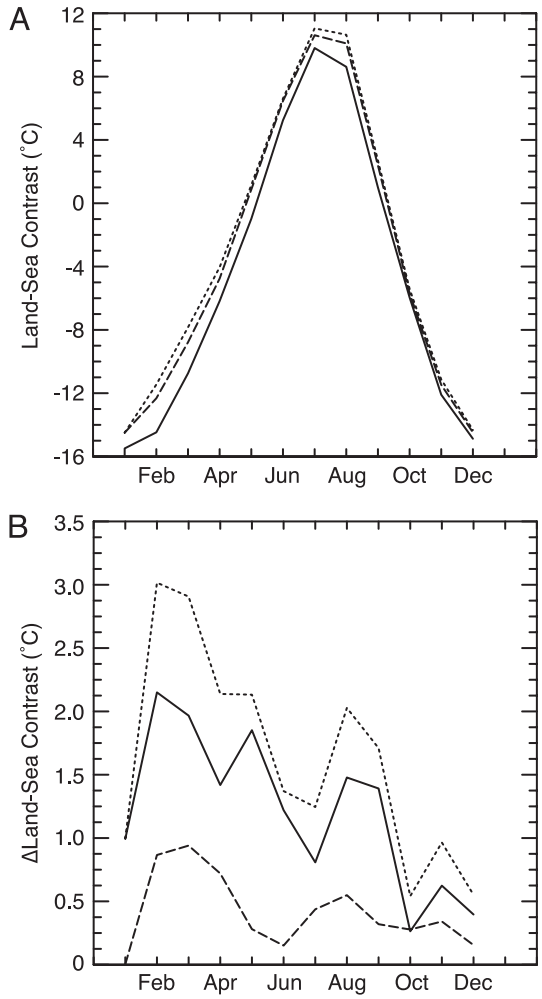

Fig. 1. Simulated land–sea temperature contrast and anomalies. (*A*) Land–sea temperature contrast (calculated as land − ocean) for the CONTROL (solid line), $2XCO_2$ (large dashed line), and $2XCO_2$ + VEG (small dashed line) cases. (*B*) Anomalies in land–sea temperature contrast calculated as $2XCO_2$ − CONTROL (solid line), $2XCO_2$+VEG − $2XCO_2$ (large dashed line), and $2XCO_2$+VEG − CONTROL (small dashed line). A buffer of eight grid points was discarded from each side of the rectangular RCM domain. Land temperatures were calculated from all RCM land grid points within this buffer. Sea temperatures were calculated from all RCM ocean grid points within this buffer.

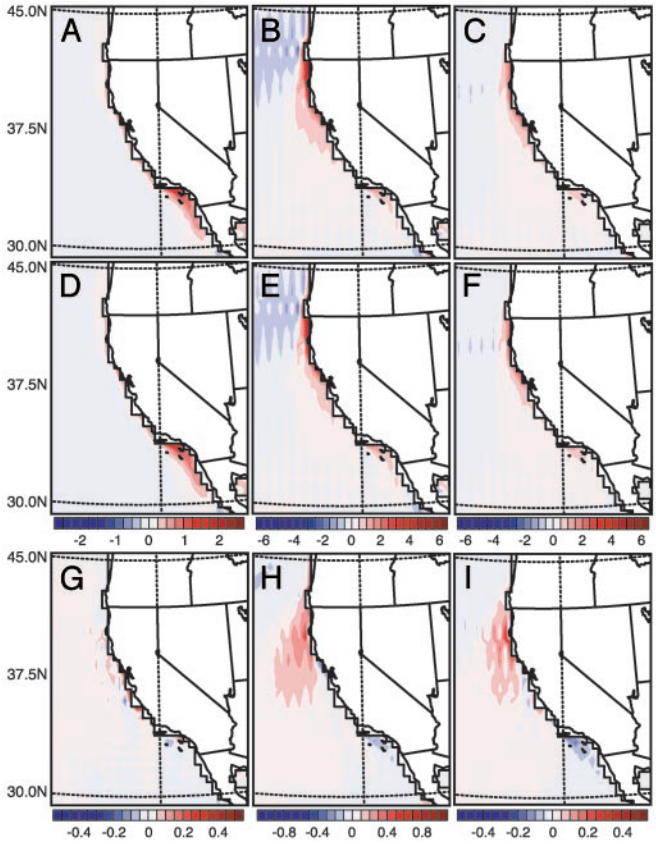

Fig. 2. Simulated California Current wind-stress curl. (*A*) May curl in the $2XCO_2$+VEG case. (*B*) August curl in the $2XCO_2$+VEG case. (*C*) September curl in the $2XCO_2$+VEG case. (*D*) May curl in the $2XCO_2$ case. (*E*) August curl in the $2XCO_2$ case. (*F*) September curl in the $2XCO_2$ case. (*G*) May curl anomalies calculated as $2XCO_2$ − CONTROL. (*H*) August curl anomalies calculated as $2XCO_2$ − CONTROL. (*I*) September curl anomalies calculated as $2XCO_2$ − CONTROL. Units are 10^{-7} N/m^3. Continental areas in the RCM are shown in white. Two coastlines are shown. The jagged line represents the RCM coastline. The smooth line represents the actual coastline. RCM grid boxes are 40 × 40 km.

albedo in both coastal and inland areas of the southern half of the model domain (data not shown). The anomalies in land–sea contrast caused by these land-cover–atmosphere feedbacks ($2XCO_2$+VEG − $2XCO_2$) are 33–50% of the value of those caused by CO_2 radiative forcing ($2XCO_2$ − CONTROL) (Fig. 1*B*). Although both CO_2 forcing and biophysical feedbacks induce positive land–sea temperature anomalies in all months, there are subtle differences in the seasonality of the respective effects, particularly during the spring–summer and summer–autumn transitions. The net result of the land-cover feedbacks is therefore not only an augmentation of the differential warming over land seen in the $2XCO_2$ case but also a change in the seasonal cycle of the land–sea contrast.

RCM-simulated wind-stress curl is shown in Fig. 2 for the $2XCO_2$ (*A–C*) and $2XCO_2$+VEG (*D–F*) cases. The change in the absolute value and seasonal structure of the land–sea contrast induced by land-cover–atmosphere feedbacks alters the magnitude and seasonal structure of wind-stress curl, and thereby upwelling, in both the northern and southern limbs of the California Current (Fig. 2 *G–I*). Positive wind-stress curl is increased in the $2XCO_2$+VEG case over the $2XCO_2$ case in the early season (March through May) by up to 180% in the northern limb and 10–15% in the southern limb (with a decrease of 15% in May in the southern limb). In the peak season (June through August), positive wind-stress curl is enhanced up to 140% in the northern limb. Decreases in July are 10% on the coast and up to 80% further from shore. In the southern limb, positive wind-stress curl is reduced 10–20% in June and August and increased 15% in July. Finally, in the late-season (September and October), positive wind-stress curl is increased by 60–140% in the northern limb and decreased up to 20% in the southern limb.

The effects of land-cover–atmosphere interactions on coastal upwelling shown in Fig. 2 accentuate the effects of CO_2 radiative forcing. The absolute values of zonally averaged wind-stress curl are shown in Fig. 3 *A–C*. As demonstrated by Snyder *et al.* (5), forcing by doubled preindustrial atmospheric CO_2 levels intensifies the upwelling season in the northern limb of the California Current while muting seasonality in the southern limb (Fig. 3*D*). CO_2-induced land-cover–atmosphere interactions also alter the seasonal and latitudinal structure of California Current wind-stress curl (Fig. 3*E*). Between 35°N and 39°N, there is a 2- to 3-month delay between maximum early-season increase in land–sea temperature contrast and the early-season increase in wind-stress curl (Figs. 1 and 3*E*). Between 37°N and 43°N, the

GEOPHYSICS

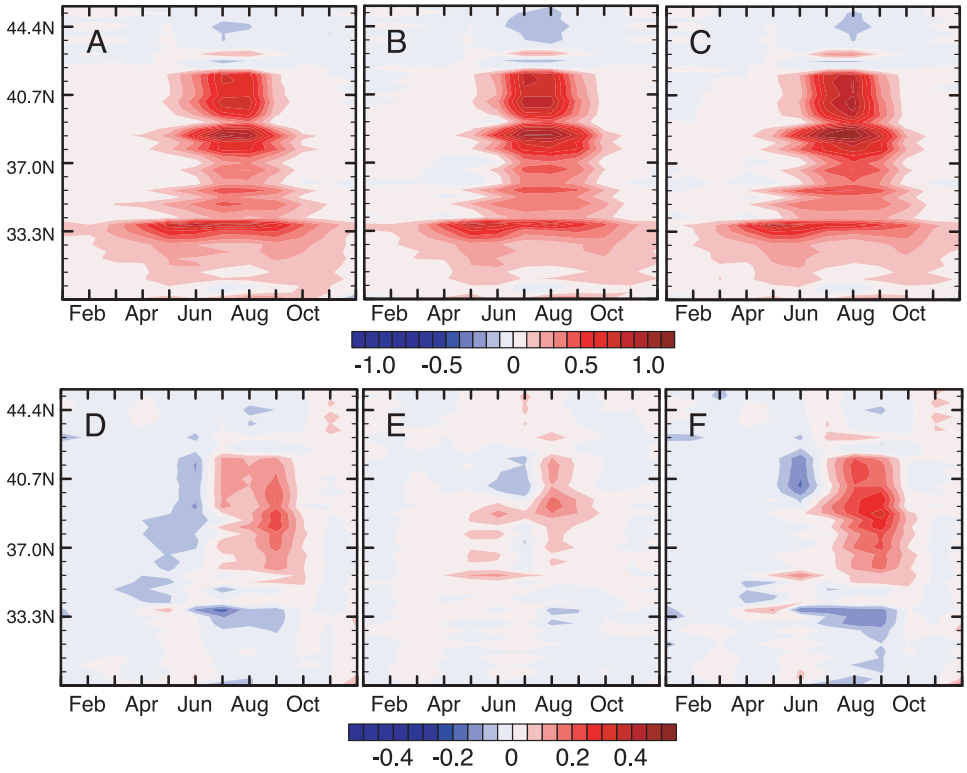

Fig. 3. Zonally averaged wind-stress curl anomalies for the California Current region. (*A*) Zonally averaged curl in the CONTROL case. (*B*) Zonally averaged curl in the $2XCO_2$ case. (*C*) Zonally averaged curl in the $2XCO_2$+VEG case. (*D*) Anomalies calculated as $2XCO_2$ − CONTROL. (*E*) Anomalies calculated as $2XCO_2$+VEG − $2XCO_2$. (*F*) Anomalies calculated as $2XCO_2$+VEG − CONTROL. Zonal averages were calculated over a band of six ocean points along the coast. Units are 10^{-7} N/m^3.

peak-season increase in wind-stress curl occurs contemporaneously with the maximum peak-season increase in land–sea temperature contrast. Overall, the land-cover–atmosphere coupling results in a positive feedback that in the northern limb further intensifies peak- and late-season wind-stress curl and in the southern limb further increases early-season wind-stress curl and further decreases peak- and late-season wind-stress curl (Fig. 3*F*).

We propose that land-cover feedbacks will generally enhance the effects of CO_2 radiative forcing on California Current activity. For the northern limb, radiative forcing decreases early-season activity and enhances peak- and late-season activity (Fig. 4). Biophysical feedbacks mitigate this early-season reduction in activity, although the total effect of radiative forcing and land-cover feedback is negative, resulting in decreased early-season upwelling relative to the modern regime. More importantly, biophysical feedbacks further intensify peak- and late-season upwelling in the northern limb, increasing both the total seasonal upwelling and the seasonal contrast of upwelling over what is seen with radiative forcing alone. In the southern limb, radiative forcing slightly increases early-season upwelling while decreasing peak- and late-season upwelling more substantially (Figs. 3 and 4). Land-cover–atmosphere feedbacks accentuate this response. Just south of the Southern California Bight (34°N), feedbacks further increase early-season activity and further decrease mid- and late-season activity, resulting in a slight phase shift in upwelling seasonality (Fig. 3). For the southern limb overall, land-cover–atmosphere feedbacks accentuate the mid- and late-season decreases in upwelling seen with radiative forcing alone, resulting in a decrease in both total-season upwelling and seasonal contrast (Fig. 4).

These biophysically induced alterations of eastern boundary current upwelling intensity and seasonality would likely impact both marine and terrestrial environments. The potential impacts of radiatively forced changes in coastal upwelling activity have been outlined elsewhere (2, 5, 23). Many of these impacts will likely be accentuated by land-cover–atmosphere feedbacks. Additionally, new impacts may also be introduced, particularly where coastal upwelling provides multiple controls on ecosystem function (24, 25) and where additional intensification by these feedbacks eclipses thresholds that would not have been surpassed in response to radiative forcing alone.

This study quantifies the effects of CO_2-induced Earth-system feedbacks on upwelling activity in eastern boundary current regions. There are a number of caveats to these results. First, it has been shown that the response of climate to land-cover change varies with atmospheric CO_2 concentration (11). The actual future manifestation of the land-cover–upwelling interactions proposed here will likely be moderated by the actual trajectory of CO_2 change and the timing of land-cover response to that change, the latter of which will likely vary among eastern boundary current regions. Second, we have considered only the response of potential vegetation to elevated CO_2. Much of the landscape in eastern boundary current regions has been altered by human activity (26–28), and anthropogenic land-cover types such as urban and cropland have likely played a substantial role in historical land-cover–upwelling interactions. A quantitative understanding of the trajectory of future human modification of the landscape (as in ref. 29), particularly how that trajectory is influenced by elevated CO_2, is necessary to fully assess the future impacts of land-cover change on coastal upwelling regimes. Third, the RCM does not explicitly simulate coastal fog. Increases in coastal upwelling could be expected to increase the coastal fog production associated with the northern limb upwelling regime, impacting fog-dependent coastal vegetation and creating biophysical feedbacks more complex than those explored here. Increased coastal fog could also serve as a negative feedback, because the high albedo of fog could decrease short-

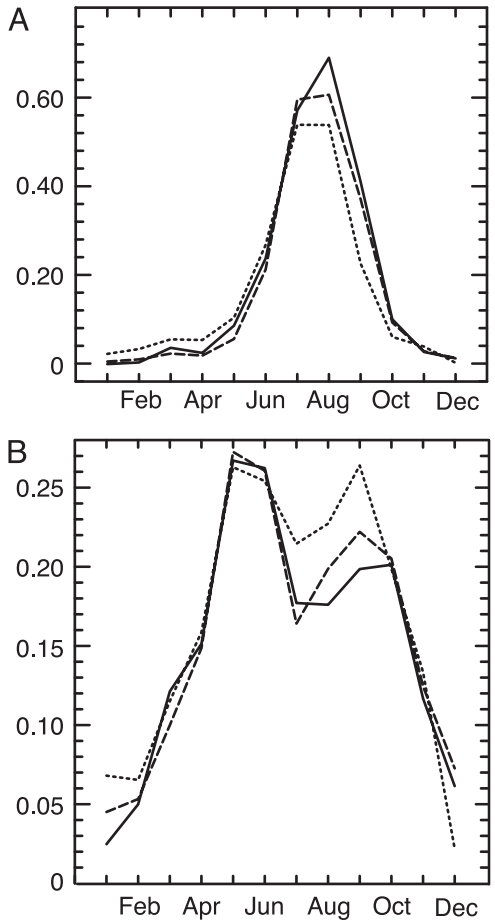

Fig. 4. Regional response of the California Current to radiative forcing and land-cover–atmosphere feedbacks. Values of wind-stress curl in the CONTROL (small dashed line), $2XCO_2$ (large dashed line), and $2XCO_2$+VEG (solid line) cases were averaged over a band of six ocean grid points along the coast. (*A*) Northern limb (34°N to 42°N). (*B*) Southern limb (29.6°N to 34°N). Latitudinal definitions of the northern and southern limbs were based on the placement of the Southern California Bight (34°N) and Capo Blanco (42.5°N) on the RCM grid (see Fig. 2).

wave radiation absorbed at the surface, mitigating coastal warming. However, the land–sea thermal contrast that drives eastern boundary currents results from seasonal heating over inland regions (30), thus the effect of coastal temperature dynamics may be minimal. Fourth, our conclusions depend on the accuracy of the climate and vegetation model simulations. Because BIOME4 is an equilibrium vegetation model, the simulated vegetation could be sensitive to the magnitude of interannual variability in the RCM integration (and thereby to the length of the RCM integration). Additionally, other climate–vegetation model couplings show very coarse changes in vegetation distribution in the western United States in response to elevated atmospheric CO_2 levels [e.g., the intercomparison of Cramer *et al*. (31)], although because these studies used general circulation models, regional dynamics were represented by only a handful of grid points. Nonetheless, because it does not include carbon–nitrogen interactions or photosynthetic down-regulation, the vegetation model used here may overestimate the physiological response of vegetation cover to increased CO_2 concentrations (see discussion in ref. 12). However, with elevated CO_2, such an error would be expected to produce increases in soil moisture and evaporation and decreases in sensible heating, the direct opposite of the response observed here.

Although our experiments have focused on biophysical feedbacks, there are other feedback mechanisms that could also alter activity in eastern boundary current regions. Bakun (2) has suggested that if primary production increases as a result of intensified upwelling, sequestration of carbon beneath the ocean thermocline should also increase, providing a negative feedback by dampening the anthropogenic increase in atmospheric CO_2 concentrations. Biogeochemical feedbacks could also occur on land, particularly if nitrogen–carbon interactions or photosynthetic down-regulation exert a negative control on plant responses to elevated CO_2 (32–34). Conversely, intensified upwelling could itself create a positive feedback by decreasing the surface temperature of the near-shore ocean, which would serve to further enhance the land–sea temperature contrast (2). Finally, it has been observed that in strong El Niño years, California Current activity is suppressed and sea surface and subsurface temperatures increase (35). The response of important modes of climate variability such as the El Niño Southern Oscillation and the Pacific Decadal Oscillation will likely also play a key role in the response of eastern boundary currents to elevated CO_2 levels. Complete assessment of the sensitivity of these important environmental systems to greenhouse warming requires understanding not only of their sensitivity to equilibrium forcing but also of their sensitivity to climate-system feedbacks affecting both the equilibrium climate state and climate-system variability.

We thank M. Huber for assistance with the wind-stress curl calculations, J. L. Bell for assistance with RegCM2.5, and P. J. Bartlein for helpful discussions of the RegCM2.5/BIOME4 coupling strategy. The insightful comments of three anonymous reviewers greatly improved the manuscript. This research was supported by the David and Lucile Packard Foundation and the ARCS Foundation.

1. Bakun, A. & Nelson, C. S. (1991) *J. Phys. Oceanogr.* **21,** 1815–1834.
2. Bakun, A. (1990) *Science* **247,** 198–201.
3. Schwing, F. B. & Mendelssohn, R. (1997) *J. Geophys. Res. Oceans* **102,** 3421–3438.
4. Mote, P. W. & Mantua, N. J. (2002) *Geophys. Res. Lett.* **29,** 2138.
5. Snyder, M. A., Sloan, L. C., Diffenbaugh, N. S. & Bell, J. L. (2003) *Geophys. Res. Lett*., 10.1029/2003GL017647.
6. Doherty, R., Kutzbach, J., Foley, J. & Pollard, D. (2000) *Clim. Dyn.* **16,** 561–573.
7. Govindasamy, B., Duffy, P. B. & Caldeira, K. (2001) *Geophys. Res. Lett.* **28,** 291–294.
8. Levis, S., Foley, J. A. & Pollard, D. (2000) *J. Clim.* **13,** 1313–1325.
9. Chase, T. N., Pielke, R. A., Kittel, T. G. F., Nemani, R. R. & Running, S. W. (2000) *Clim. Dyn.* **16,** 93–105.
10. Claussen, M., Brovkin, V. & Ganopolski, A. (2001) *Geophys. Res. Lett.* **28,** 1011–1014.
11. Pitman, A. J. & Zhao, M. (2000) *Geophys. Res. Lett.* **27,** 1267–1270.
12. Diffenbaugh, N. S., Sloan, L. C., Snyder, M. A., Bell, J. L., Kaplan, J. O., Shafer, S. L. & Bartlein, P. J. (2003) *Global Biogeochem. Cycles*, 10.1029/2002GB001974.
13. Bell, J. L., Sloan, L. C. & Snyder, M. A. (2004) *J. Climate* **17,** 81–87.
14. Ryther, J. H. (1969) *Science* **166,** 72–76.
15. Thompson, R. S., Anderson, K. H. & Bartlein, P. J. (1999) *Atlas of Relations Between Climatic Parameters and Distributions of Important Trees and Shrubs in North America* (US Geological Survey, Denver), Professional Paper 1650 A and B.
16. Kiehl, J. T., Hack, J. J., Bonan, G. B., Boville, B. A., Williamson, D. L. & Rasch, P. J. (1998) *J. Clim.* **11,** 1131–1149.
17. Giorgi, F. & Shields, C. (1999) *J. Geophys. Res. Atmos.* **104,** 6353–6375.
18. Snyder, M. A., Bell, J. L., Sloan, L. C., Duffy, P. & Govindasamy, B. (2002) *Geophys. Res. Lett*., 10.1029/2001GL014431.
19. Diffenbaugh, N. S., Sloan, L. C. & Snyder, M. A. (2003) *Paleoceanography*, 10.1029/2002000865.
20. Kaplan, J. O. (2001) in *Department of Ecology* (Lund University, Lund, Sweden), pp. 128.
21. de Noblet-Ducoudré, N., Claussen, R. & Prentice, C. (2000) *Clim. Dyn.* **16,** 643–659.
22. Dickinson, R. E., Henderson-Sellers, A. & Kennedy, P. J. (1993) *Biosphere-*

Atmosphere Transfer Scheme (BATS) Version 1e as Coupled to the NCAR Community Climate Model (National Center for Atmospheric Research, Boulder, CO).
23. Soto, C. G. (2001) *Rev. Fish Biol. Fish.* **11,** 181–195.
24. Agostini, V. N. & Bakun, A. (2002) *Fish. Oceanogr.* **11,** 129–142.
25. Bakun, A. (1996) *Patterns in the Ocean: Ocean Processes and Marine Population Dynamics* (California Sea Grant College System, National Oceanic and Atmospheric Administration, in cooperation with Centro de Investigaciones Biológicas del Noroeste, La Jolla, CA).
26. Ramankutty, N. & Foley, J. A. (1999) *Global Biogeochem. Cycles* **13,** 997–1027.
27. Olson, J. S., Watts, J. A. & Allison, L. J. (1983) *Carbon in Live Vegetation of Major World Ecosystems* (Oak Ridge National Laboratory, Oak Ridge, TN).
28. Loveland, T. R., Reed, B. C., Brown, J. F., Ohlen, D. O., Zhu, Z., Yang, L. & Merchant, J. W. (2000) *Int. J. Remote Sens.* **21,** 1303–1330.
29. Fischer, G. & Sun, L. X. (2001) *Agric. Ecosyst. Environ. Appl. Soil Ecol.* **85,** 163–176.
30. Huyer, A. (1983) *Prog. Oceanogr.* **12,** 259–284.
31. Cramer, W., Bondeau, A., Woodward, F. I., Prentice, I. C., Betts, R. A., Brovkin, V., Cox, P. M., Fisher, V., Foley, J. A., Friend, A. D., *et al.* (2001) *Global Change Biol.* **7,** 357–373.
32. Shaw, M. R., Zavaleta, E. S., Chiariello, N. R., Cleland, E. E., Mooney, H. A. & Field, C. B. (2002) *Science* **298,** 1987–1990.
33. Gill, R. A., Polley, H. W., Johnson, H. B., Anderson, L. J., Maherali, H. & Jackson, R. B. (2002) *Nature* **417,** 279–282.
34. Huxman, T. E., Hamerlynck, E. P., Moore, B. D., Smith, S. D., Jordan, D. N., Zitzer, S. F., Nowak, R. S., Coleman, J. S. & Seemann, J. R. (1998) *Plant Cell Environ.* **21,** 1153–1161.
35. Simpson, J. J. (1983) *Geophys. Res. Lett.* **10,** 937–940.